JOURNAL OF GEOPHYSICAL RESEARCH, VOL. 114, B10204, doi:10.1029/2009JB006339, 2009

Organization of volcanic plumbing through magmatic lensing by magma chambers and volcanic loads

Leif Karlstrom,[1] Josef Dufek,[2] and Michael Manga[1]

Received 29 January 2009; revised 23 April 2009; accepted 14 July 2009; published 10 October 2009.

[1] The development of discrete volcanic centers reflects a focusing of magma ascending from the source region to the surface. We suggest that this organization occurs via mechanical interactions between magma chambers, volcanic edifices, and dikes and that the stresses generated by these features may localize crustal magma transport before the first eruption occurs. We develop a model for the focusing or "lensing" of rising dikes by magma chambers beneath a free surface, and we show that chambers strongly modulate dike focusing by volcanic edifices. We find that the combined mechanical effects of chambers, edifice loading, and dike propagation are strongly coupled. Chambers deeper than ~20 km below the surface with magmatic overpressure in the range of 20–100 MPa should dominate dike focusing, while more shallow systems are affected by both edifice and chamber focusing.

Citation: Karlstrom, L., J. Dufek, and M. Manga (2009), Organization of volcanic plumbing through magmatic lensing by magma chambers and volcanic loads, *J. Geophys. Res.*, *114*, B10204, doi:10.1029/2009JB006339.

1. Introduction

[2] The presence of volcanic edifices requires a focusing of magma ascending from the mantle and lower levels of the crust. The spatial extent and processes of magma transport beneath volcanoes that govern the discrete morphology and spacing of volcanic centers are, however, difficult to constrain because the transport network is buried beneath the surface, and it evolves on timescales that range from hours (volcanic eruptions [e.g., *Stasuik et al.*, 1993; *Petcovic and Dufek*, 2005]) to $\sim 10^6$ years (crustal melt flux [e.g., *Dimalanta et al.*, 2002; *Dufek and Bergantz*, 2005]).

[3] Melt ascending from the upper mantle must negotiate structural controls imposed by material and rheological boundaries within the crust, as well as an increasingly cool thermal environment, that act to slow and sometimes stall magma ascent. In addition, tectonic stresses and near-surface faults may often play a significant and location-specific role in the organization of volcanism [e.g., *Nakamura et al.*, 1977; *Vigneresse et al.*, 1999]. These background features determine the environment through which magma migrates, and may influence the locations of deep-seated magma chambers [e.g., *Kavanagh et al.*, 2006] as well as the pathways available to volcanism [e.g., *Galland et al.*, 2007]. Within the confines of these initial conditions, the processes of magma transport organize the volcanic plumbing system into discrete centers that then are expressed as volcanoes on the surface. These centers in turn affect the background state of the crust, and represent thermomechanical anomalies that will exert increasingly long-range influence over their active lifetimes.

[4] Two general approaches are typically followed to explain the formation and evolution of volcanic centers. These take either a "bottom up" or "top down" perspective, whereby processes occurring at the melt source region or at the surface dominate the organization and focusing of rising magma. Implicit in both approaches is the assumption that boundary conditions at the top or bottom interface of the transport region dominate internal dynamics. The top down models account for the effect of volcano building on the stress state in the underlying crust [e.g., *Pinel and Jaupart*, 2000; *Muller et al.*, 2001], and the role of lithospheric flexure in the formation and subsequent organization of volcanoes [*ten Brink*, 1991; *Hieronymus and Bercovici*, 1999]. Volcano loading and resulting flexural stresses can have a significant effect on subsurface processes, though it is of note that all top down studies to date require the presence of an initial volcano to focus magma. Bottom up models [e.g., *Marsh and Carmichael*, 1974; *Olson and Singer*, 1985; *Ihinger*, 1995], on the other hand, establish discrete volcanic centers much earlier in the transport network. Here, fluid dynamic instabilities (Rayleigh-Taylor type) generate zones of enhanced melting in the mantle source region; subsequent ascent and eruption of these melts generates edifice spacing corresponding to the spacing of the melting zones.

[5] There is, however, an additional possibility for the organization of a magma plumbing system, in which localization occurs intermediate to the "top" and "bottom" regions, prior to the first eruption. It has been recognized that individual components of the magmatic transport system (dikes, chambers) can significantly alter the mechanical and thermal properties of their surroundings [e.g., *Ito and Martel*, 2002; *Jellinek and DePaolo*, 2003; *de Silva and*

[1]Department of Earth and Planetary Sciences, University of California, Berkeley, California, USA.
[2]School of Earth and Atmospheric Sciences, Georgia Institute of Technology, Atlanta, Georgia, USA.

0148-0227/09/2009JB006339$09.00

Gosnold, 2007]. Here we show that localization via surface or source boundary conditions are end-member cases for the formation of volcanic centers, and that magmatic plumbing systems may be actively self-organized in the subsurface through interactions between magma chambers and dikes in addition to volcanic edifices. These focusing processes are not mutually exclusive, nor are they necessarily part of a mechanistic hierarchy. Rather, interfacial, structural, and internal dynamic controls on magmatic localization form the basis of a general physical framework for understanding volcanic centers.

[6] We propose a new addition to this framework, and develop a simple static model of dike focusing due to an overpressured and buoyant magma chamber beneath a free surface. This chamber growth mechanism (hereafter referred to as ''magmatic lensing'') is an effective way to localize rising magma, and we show that it may dominate the static effects of surface loading in many cases. Temporal evolution of the mechanical system, including thermally induced rheological modulation of crustal stresses and chamber rupture are not considered here, but are the subject of a companion paper (L. Karlstrom et al., Magma chamber stability in arc and continental crust, submitted to *Journal of Volcanology and Geothermal Research*, 2009) that considers the stability of magma chambers that grow via dike focusing. Magmatic lensing is a process that has implications for the formation of magmatic plumbing, and extends previously proposed ideas for the formation of discrete volcanic centers.

[7] As a qualitative application of our model, we then show how the spacing of magma chambers controlled by magmatic lensing might be used to interpret arc volcano spacing, and to constrain chamber sizes and depths. We compile a database of spacing between discrete Holocene stratovolcanoes around the Pacific Rim, and show that the observed average spacing between centers may be produced in our model by dike-lensing magma chambers. We are unable to uniquely constrain chamber depth or size, but show that chambers at mid to lower crustal depths with a range of volumes fit the observational data equally well. We find that circum-Pacific volcano spacing is not correlated with plate convergence rate or crustal thickness (for crust thicker than 20 km), consistent with the idea that long-term magma storage modulates spacing. Based on our calculations and observations of Pacific Rim arc volcanoes, we hypothesize that volcanic plumbing is a self-organizing system that evolves to a given surface morphologic expression constrained, but not solely determined, by the surface and source region boundary conditions.

2. Methods

[8] We model a magma chamber in two spatial dimensions as a pressurized and buoyant cylindrical cavity in an elastic half-space [e.g., *Odé*, 1957; *Gudmundsson*, 2006], as depicted in Figure 1. This model is static, in that we do not directly address dike propagation or time-dependent stresses such as might arise from viscoelastic or yielding rheology, and we neglect any buoyant rise of the magma chamber. However, even in the lower crust dike propagation timescales should be shorter than both the viscoelastic relaxation timescale of the country rock and the Stokes risetime of the chamber (Karlstrom et al., submitted manuscript, 2009), and evidence of pervasive diking in mid to lower crustal terrains (10–25 km depth) [e.g., *Dumond et al.*, 2007] provides observational support for the assumption of some elastic behavior at depth. As our present purpose is to compare the mechanical properties of magmatic lensing to other melt focusing proposals at a range of depths, such a simple analysis is justified. In this level of analysis, we also neglect depth-dependent density [*Grosfils*, 2007], and the more complicated chamber geometries inferred for real volcanic systems [e.g., *Newman et al.*, 2006].

[9] Solutions are obtained to the equations of linear elasticity by the method of stress functions [*Fung*, 1965]. Boundary conditions at the chamber wall are

$$\sigma^n = \Delta P + \Delta\rho g R \cos\phi \tag{1}$$

$$\sigma^t = 0 \tag{2}$$

and at the free surface $y = 0$

$$\sigma^n = 0 \tag{3}$$

$$\sigma^t = 0 \tag{4}$$

where σ^n is the normal stress and σ^t is the tangential stress, ΔP is the chamber pressure over lithostatic, $\Delta\rho$ is the density difference between magma and the country rock, R is the radius of the chamber, g is gravity and $r\cos\phi = y$ defines the polar coordinate system used to write down boundary condition equation (1) (Figure 1). Using the bipolar coordinate system [e.g., *Jeffery*, 1921], we obtain approximate stress functions (detailed in Appendix A) from which displacements and deviatoric stresses may be determined. We use the convention that positive stresses are compressive.

[10] To evaluate the influence of a volcanic edifice for which an analytic solution is not possible, we calculate stresses due to a chamber and a triangular surface load with the Direct Boundary Integral code BEMECH [*Gao and Davies*, 2002]. We discretize the free surface with 150 quadratic boundary elements extending 5000 times the volcano width to approximate an infinite boundary, and use exponential node spacing near the corners of the volcanic edifice to more accurately resolve the load; the edifice is exponentially discretized with 23 elements. The surface satisfies the boundary conditions

$$\sigma^n = \begin{cases} \rho_b g h \frac{(w-|x|)}{w} & \text{if } -w \le x \le w \\ 0 & \text{otherwise} \end{cases} \tag{5}$$

$$\sigma^t = 0 \tag{6}$$

with h the height of the volcano, w its half width, and $\rho_b = 3000$ kg/m^3 an upper bound for density (Figure 1). The circumference of the magma chamber is described by 176

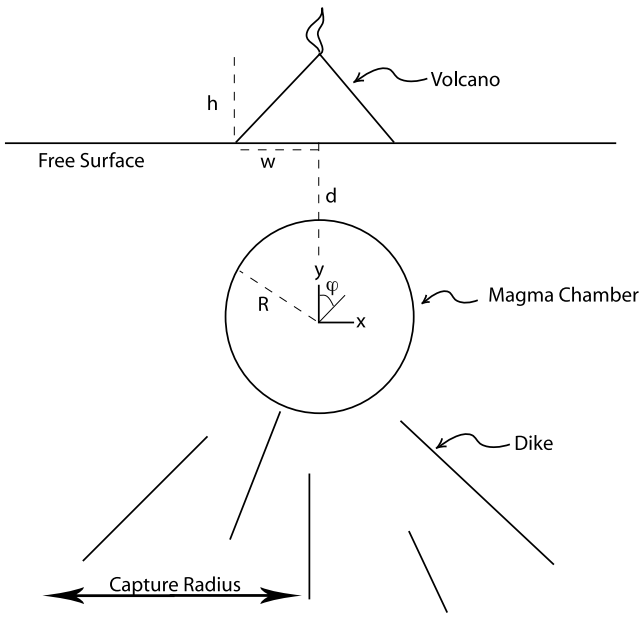

Figure 1. Geometry of the model problem. A circular magma chamber, overpressured and buoyant with respect to its surroundings, lies beneath a volcano sitting on an otherwise free surface. Chamber stresses focus rising dikes from a region defined by the magnitude of principal deviatoric stresses around the chamber. The capture radius of the chamber is the horizontal extent of this region, defined at a given depth below the chamber.

uniformly spaced quadratic boundary elements. We assume a lithostatic background stress field for the simulations here, but do address the qualitative effects of regional deviatoric tectonic stress, a possible scenario in many realistic circumstances [e.g., *Muller et al.*, 2001]. Mesh refinement does not change our results significantly, and comparison with available analytical solutions for the case of no edifice (equations (A12)–(A14)) confirms the accuracy of the method.

3. Magmatic Lensing

[11] The magma chamber is supplied by melt contained in rising dikes, and represents a location where migrating magma stalls or accumulates. We assume that dikes propagate in a direction perpendicular to the least compressive principal stress at the dike tip [e.g., *Anderson*, 1951]. Dikes are often modeled as two-dimensional fluid filled mode I fractures driven by overpressure and buoyancy [*Rubin*, 1995a]. Dikes propagate, in the most general sense, when the potential energy released through propagation is sufficient to fracture rock at the crack tip [*Griffith*, 1920]. This is a threshold energy criterion for propagation, and is a feature of all "critical" dike propagation models, though so-called "subcritical" dike propagation [*Atkinson and Meredith*, 1987] may also be an important magma transport mechanism over short distances [*Chen and Jin*, 2006].

[12] We use the less general but more convenient stress intensity factor formulation of linear elastic fracture mechanics [e.g., *Rubin*, 1995b], from which the simplest model of a dike is derived: a uniformly pressurized elliptical crack that propagates when the stress intensity factor K exceeds the critical value $K \geq K_{crit} = \Delta P_{dike} \sqrt{L}$. Here K_{crit} is the critical stress intensity factor or fracture toughness of the host rock, ΔP_{dike} is the dike overpressure, and L is the length of the dike. We take $K_{crit} = 10^6$ Pa $m^{1/2}$ [*Rubin*, 1995b], with the understanding that this value is not well constrained for crustal materials, and may vary dike to dike as well as with depth [e.g., *Atkinson and Meredith*, 1987]. Therefore, the threshold stress for dike propagation in our model is 10^6 Pa (but see below), and far-field deviatoric principal stresses in excess of this value may reorient the trajectory of a rising dike.

[13] It should be emphasized that our threshold approach is a simplification because the evolving stress field generated by the dike itself must be accounted for to determine the true propagation direction. Indeed, a detailed numerical calculation of dike propagation from volcanic centers [*Mériaux and Lister*, 2002] reveals that calculation of dike trajectories solely from the ambient stress field may be inaccurate. Nevertheless, *Mériaux and Lister* [2002] show that the qualitative aspects of dike reorientation remain unchanged, and that magmatic lensing effects may even be amplified when the more detailed mechanics are included. The reorientation of dikes has been found to be significant even when more geometrically detailed propagation is accounted for [*Muller et al.*, 2001], and more realistic ellipsoidal chamber geometries [e.g., *Gudmundsson*, 2006] do not affect the first-order stresses. Some treatments of dike propagation neglect the strength of crustal rocks [e.g., *Pinel and Jaupart*, 2000], on the grounds that its contribution to the overall force balance is negligible. We note, however, that processes occurring at the dike tip still control the propagation direction, and that any other critical dike model will also contain a threshold driving stress criteria for propagation.

[14] Our approach is a class of parameterization that captures the physics of interest. We expect our results to be most accurate in the limiting case when chamber stresses are much larger than dike stresses, a situation that may be typical (see section 6) even though dike overpressures (determined by dike length and buoyancy) may vary. We also expect that our choice of 1 MPa as a threshold stress for dike reorientation is an upper bound, as the fully coupled problem reveals that dikes may be much more easily affected by background deviatoric stresses [*Mériaux and Lister*, 2002]. Our criteria for dike reorientation should thus provide a conservative estimation of magmatic lensing.

[15] For chambers that are significantly overpressured or buoyant with respect to regional stresses there exists a region below the chamber inside which stresses are larger than the critical stress of 1 MPa, and trajectories of rising dikes are focused toward the magma chamber (Figure 1). We quantify this region through the notion of a "capture radius" at a given depth below the magma chamber, measured from the center of the chamber parallel to the free surface (Figures 1 and 2a), and defined by the distance for which chamber stresses are large enough to affect rising dikes. Because chamber stresses fall off rapidly in magnitude away from the chamber, this capture radius depends on the depth at which it is evaluated (Figure 2b), and we

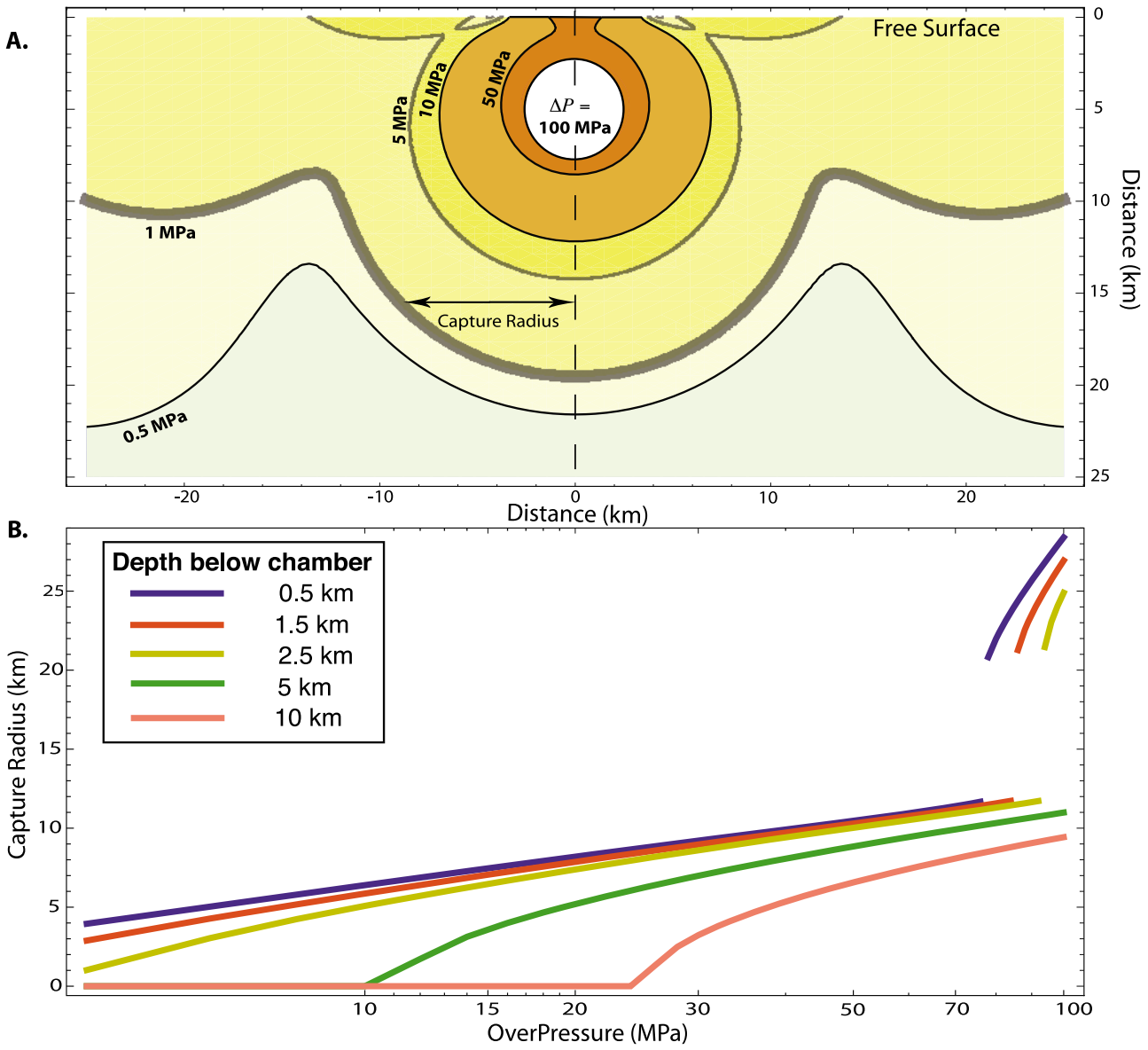

Figure 2. (a) Contours of least compressive deviatoric principal stress around a 2.5 km radius chamber at 5 km depth below the surface. $\Delta P = 100$ MPa, and $\Delta\rho = 300$ kg/m^3. The region in which dikes may be affected by chamber stresses is shown with a thick grey contour. This region defines the capture radius, which is shown at 10 km below the chamber. (b) Capture radius as a function of chamber overpressure, for the geometry depicted in Figure 2a. Note that capture radius depends on depth below the chamber and that (for this example) depths of <2.5 km below the chamber experience a discontinuous increase in capture radius (see text). A smaller threshold stress (here set to 1 MPa) will result in a significantly larger capture radius.

arbitrarily choose 10 km below the chamber as the depth at which we evaluate dike capture.

4. Magma Chamber Overpressure

[16] The importance of magmatic lensing depends critically on the magnitude of stresses exerted by the magma chamber, but bounds for chamber stresses are poorly constrained. Chamber overpressure develops through a variety of processes that include volatile exsolution, magmatic differentiation, melting or solidification of wall rocks, and injection of new magma into the chamber [e.g., *Tait et al.*, 1989; *Folch and Marti*, 1998; *Annen and Sparks*, 2002]. Of these, the largest elastic pressures ΔP are generated through injection of largely incompressible magma through dikes or melting of wall rocks, and follow

$$\Delta P = \frac{1}{\beta}\frac{\Delta V}{V} \tag{7}$$

where ΔV is the change in chamber volume V and $\beta \sim 10^{-11}$ Pa^{-1} is the magma compressibility [*Tait et al.*, 1989]. Because the initial generation of melt (with $\Delta V/V = (1.1 - 1.15)$ V upon melting [e.g., *Rapp and Watson*, 1995]) may

induce enormous pressures through equation (7) (modulated heavily by anelastic processes such as compaction, and porosity shock waves dues to permeability contrasts in the magma source region [e.g., *Spiegelman*, 1993]), dikes that remain at high melt fraction during propagation should very often have higher pressure than magma chambers. An upper bound on magma chamber overpressure in this case is given by the stress at which chamber rupture occurs, resulting in a draining of magma from the chamber, and a decrease of chamber overpressure (also following equation (7)).

[17] However, the mechanisms by which chamber rupture occurs are not well understood. A number of studies [e.g., *Sartoris et al.*, 1990] use the criterion that chamber rupture occurs when tensile stresses at the wall of the chamber exceed the tensile strength of rocks. This leads to maximum overpressures on the order of 1–10 MPa, for laboratory-determined values of rock failure [*Atkinson and Meredith*, 1987; *Gudmundsson*, 1988]. This is likely an underestimate of maximum chamber overpressure at depth, which may also be a function of tectonic regime, as rock failure depends on confining stresses and background deviatoric stresses. The rheology of magma chamber wall rocks will be strongly affected by prolonged heating, and thus critical brittle fracture may not be the dominant mode of initial chamber rupture. Anelastic processes, such as the viscous blunting of dike tips, and viscoelastic relaxation of deviatoric stresses around the chamber have been shown to strongly affect the initiation and propagation of cracks [e.g., *Dragoni and Magnanensi*, 1989; *Jellinek and DePaolo*, 2003; *Chen and Jin*, 2006]. However, these processes are not straightforward to quantify, so other criteria are currently more reliable for estimating maximum chamber overpressures.

[18] Thermal considerations of long-distance dike propagation by *Rubin* [1995a] have been used to place bounds on pressures needed to drive a dike from magma chamber to surface [*Jellinek and DePaolo*, 2003]. By balancing the elastic propagation of a dike and the gradual solidification of dike walls, critical driving magma chamber pressures are 10–100 MPa for a range of material properties. This critical overpressure depends on the composition and tectonic setting of the chamber [*Jellinek and DePaolo*, 2003] and provides an upper bound on the driving pressures needed for propagating dikes to overcome the geothermal gradient (avoid freezing) between chamber and surface.

[19] Another approach to estimating chamber overpressure comes from volcano geodesy, where ground deformation in volcanic areas due to inflating magma chambers can be measured. Geodetic measurements of this kind are now standard at many active volcanoes worldwide [e.g., *Massonnet et al.*, 1995; *Pritchard and Simons*, 2004; *Yun et al.*, 2006], and provide estimates for the theoretical chamber overpressure necessary to produce observed ground deformation. While strongly model-dependent, there are some examples which may be used with reasonable confidence to be representative of true chamber overpressures. In particular, *Newman et al.* [2001, 2006] estimate magmatic overpressure in the Long Valley Caldera over a several year period using a viscoelastic magma chamber model, and find that geodetic data are well fit for overpressures in the range of 10–70 MPa, depending on the chamber model geometry. These pressures are not an upper bound on chamber overpressure, as the Long Valley Caldera did not erupt during the period of observation. It is of note that a purely elastic model also fit the data but required overpressures of up to 500 MPa, several times lithostatic pressure [*Newman et al.*, 2001], a result that is common in studies that use solely elastic models. Such high overpressures are unrealistic for long-term deformation, but may be possible as transient overpressure before rupture. N. Houlie et al. (Stress preconditioning and magma chamber pressure evolution at Piton de la Fournaise, submitted to *Earth and Planetary Science Letters*, 2009) combine seismicity and geodesy to infer a time series of magma chamber pressure at La Piton de la Fournaise volcano that exceeds 100 MPa (and lithostatic pressure) on several occasions over a 20 year period.

[20] We can assume, based on these observations, that magma chamber overpressure can grow quite large, during the inflation period prior to eruption. We use 100 MPa as a large but not unreasonable upper bound for magma chamber overpressure, and acknowledge that there is significant uncertainty in this quantity. We also quantify the magmatic lensing mechanism for lower magma chamber overpressure (Figure 7). However, as chamber inflation is to first approximation due to influx of magma, magmatic lensing constitutes a positive feedback (larger overpressures generated by magma influx result in a larger capture radius) that provides a means for magma chambers to attain the largest possible overpressure. We also note that once chamber rupture occurs and magma leaves the chamber, overpressure will rapidly decrease according to equation (7).

5. Results

[21] For a magmatic plumbing system containing a chamber but no surface volcanic edifice, the capture radius at any depth may be calculated implicitly by setting the maximum deviatoric principal stress equal to the critical stress of 1 MPa. Figures 3 and 4 show details of the analytic solution. We observe that for overpressure in the range of 10–100 MPa and chamber depths from 5 to 30 km below the surface, the capture radius is much larger than the chamber radius (set for the purposes of illustration to 3.5 km in Figure 3). The capture radius may exceed 10 times the chamber radius for overpressures under our estimation of maximum possible overpressure (100 MPa). This suggests that magmatic lensing may be a first-order transport process whenever an overpressured inclusion dominates the local stress field. We also observe that the presence of a free surface has a profound effect on the magnitude of principal stresses for shallow chambers. Whereas the stresses around a two dimensional chamber in an infinite medium fall off as $\Delta P/r^2 + \Delta\rho\, g/r \approx \Delta P/r^2$ (because overpressures are likely several orders of magnitude larger than buoyancy effects), the stress-free boundary acts to concentrate deviatoric principal stresses near the surface on the sides of the chamber, and reflect these stresses below the chamber.

[22] Surface stress reflection has important consequences for the initiation of dikes from a magma chamber [*Pinel and Jaupart*, 2003], and for shallow chambers it results in a dramatic increase in capture radius at depth (Figures 3 and 4). The seemingly discontinuous capture radius at 5 km depth in Figure 3 is due to the particular choice of 1 MPa for the

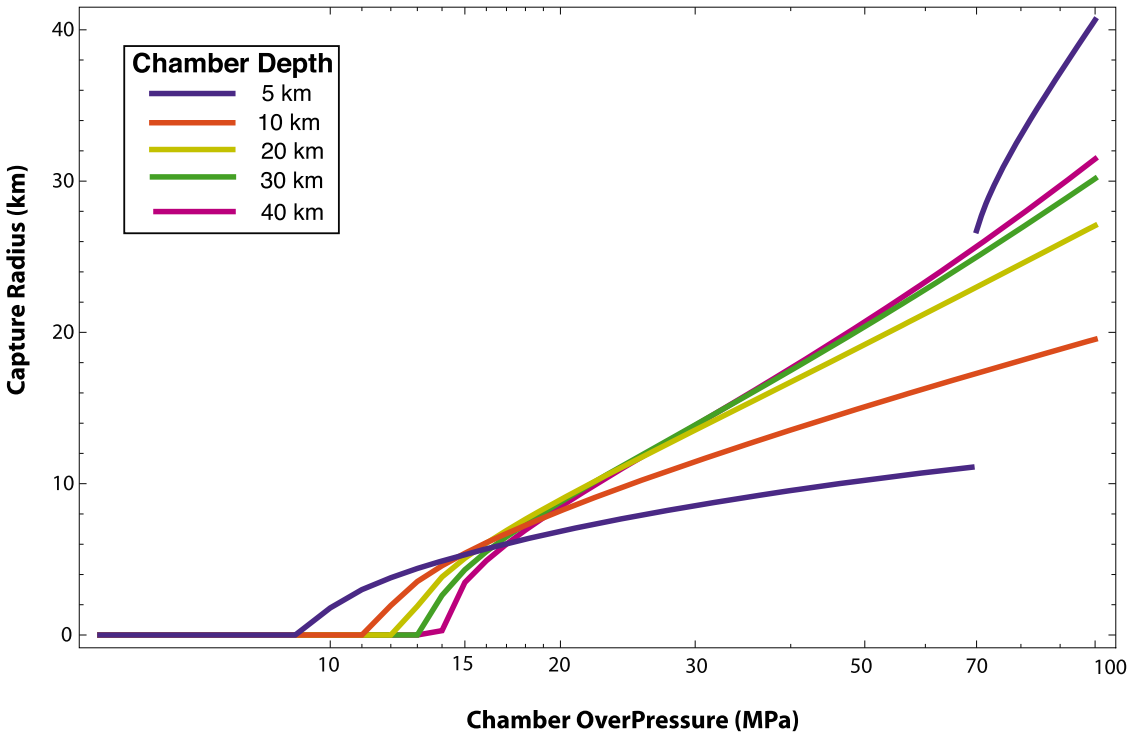

Figure 3. Capture radius as a function of overpressure for a chamber with no edifice load. Chamber radius is set to 3.5 km, and buoyancy is set to $\Delta\rho$ = 300 kg/m^3. The capture radius is evaluated 10 km below the center of the chamber (see Figure 2), for five example depths. The discontinuity present for the 5 km depth chamber is a result of this particular choice of chamber radius and is not present for chamber radii <3 km. See Figure 4 for details of a larger parameter space and the text for discussion of this surface reflection of deviatoric stresses.

threshold "critical stress" of dike capture, as well as the size of the chamber, and occurs much more dramatically for less conservative estimates of dike capture. An expanded parameter space is represented in Figure 4, where two choices of critical stress are plotted as isosurfaces, varying chamber depth and chamber radius. Figure 4 contains the information in Figures 3 and 2 as a subset of a higher-dimensional depiction of the parameter space. It also summarizes important features of the analytical solution, equations (A12)–(A14), relevant to magmatic lensing. Capture radius at 10 km depth below the chamber (Figure 2a) may be directly read off of Figure 4 by fixing chamber radius and depth, then traversing along the distance axis from 0 km until the critical stress surface of interest is reached. This distance is the capture radius for these parameters. For example, from Figure 4, a 2.5 km radius chamber at 5 km depth has a capture radius of ~10–15 km if the critical stress is 1 MPa (as used in this paper, and represented by the blue isosurface), whereas it would have a capture radius of ~50 km for a critical stress of 0.2 MPa (upper orange isosurface). In this way, the particular choice of threshold chamber stress strongly affects the capture radius (compare blue 1 MPa isosurface to orange 0.2 MPa isosurface in Figure 4). For shallow chambers, deviatoric principal stresses are concentrated in lobes on either side of the chamber (Figure 4): the imposition of a stress threshold produces a seemingly discontinuous increase in capture radius as chamber depth decreases and overpressure increases (e.g., Figures 3 and 2b). At first glance it might appear that because of the stress reflection, shallow chambers exert a stronger influence on rising dikes than deeper chambers (Figure 4, orange surface). However, as capture radius is a function of overpressure and a choice of critical stress, different choices of these parameters can result in the opposite dependence (Figure 4, lower blue surface and Figure 3).

[23] The effect of an edifice is quantified using a triangular normal load with a density of 3000 kg/m^3. We chose 2 representative triangular volcano shapes to demonstrate the effect of edifice loading on magmatic lensing: one that is 2 km across and 1 km high, and one that is 4 km across and 1 km high. These are not meant to fit all real volcanoes, but illustrate concentrated versus more broadly dispersed surface loading. They are comparable to lower density Cascade Volcanic Arc volcanoes, which are of course not triangles and not two dimensional [*Hildreth*, 2007]. Figure 5a shows the greatest principal deviatoric stress field due to the edifice loading alone, along with eigenvectors depicting approximate dike trajectories. As shown by *Muller et al.* [2001], a volcanic edifice alone may capture rising dikes, because load-induced stresses decay with depth approximately as $1/r$ (the limiting case of a surface line load, "Flamant's solution" [*Fung*, 1965]).

[24] However, the presence of a pressurized and buoyant magma chamber below an edifice changes the overall stress landscape significantly. In this case, principal deviatoric stresses at the top boundary of the chamber are opposite in sign to the edifice stresses and there is a resulting cancellation: this is a fully coupled problem, and the resulting far-field stresses are hence different than those predicted by either limiting case. Figure 5 graphically

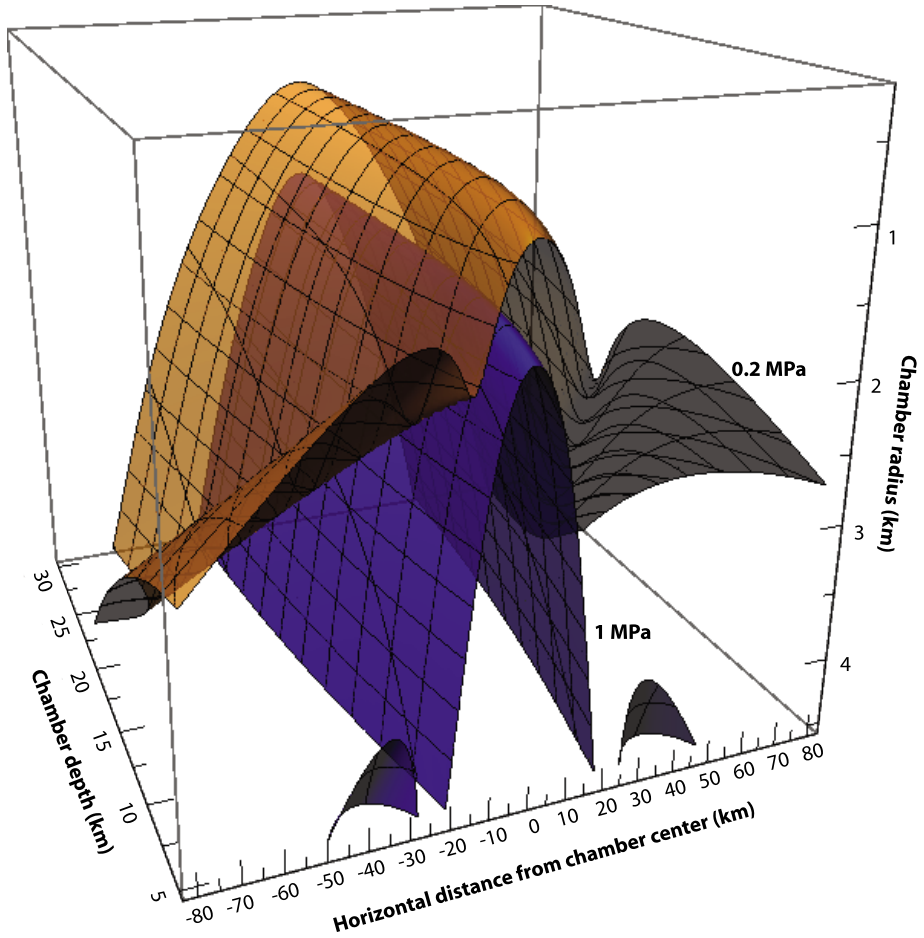

Figure 4. Isosurfaces of greatest principal deviatoric stress from equations (A12)–(A14), to illustrate how varying chamber size and depth affects the capture radius 10 km below the chamber. The upper orange surface corresponds to 0.2 MPa, and the lower blue surface corresponds to 1 MPa, representing different theoretical choices of threshold deviatoric stress needed to focus rising dikes. Axes are chamber depth, chamber radius, and horizontal (x coordinate in Figure 1) distance from the chamber center. Holding chamber depth and radius constant, the chamber's capture radius may be found by traversing from 0 to 1 of the isosurfaces and reading off the horizontal distance at which this occurs. Note the increase in capture radius for large shallow chambers ("lobes" on the blue and orange surfaces), and the effect of smaller threshold stresses for dike capture.

illustrates details of these mechanical interactions. Figure 5c shows the greatest principal deviatoric stress field due to a chamber and a compressive edifice load (least principal deviatoric stress magnitudes are exactly equal but opposite in sign), a model for the stresses due to a relatively small volcano (2 km wide by 1 km high) with a 2 km radius magma chamber beneath it. By comparing this to the case of no edifice load (Figure 5b) it is clear that, particularly in the region between the chamber and the surface, a direct cancellation of stresses has occurred (however, normal stresses for the case in Figure 5c do not exhibit this cancellation). In contrast, Figure 5d depicts the stresses due to the combined effects of a chamber and a tensile edifice load. While this particular geometry does not have a direct geological interpretation, it is meant to illustrate the force balance: deviatoric stress gradients due to the load and chamber are in the same direction between the load and the chamber, so the magnitude of the combined stresses in this region are larger than those of a chamber alone. It is also interesting to note that the stress trajectories for the volcano-chamber system focus toward the edifice and a central conduit system. This implies that surface eruptions most likely occur from within the volcano, consistent with observations and the theoretical results of others [*Pinel and Jaupart*, 2003], although the vent locations may move toward the base of the edifice if a central conduit is not well established [*Kervyn et al.*, 2009].

[25] By varying chamber radius and depth with constant edifice load, overpressure and buoyancy, we evaluate the capture radius of the combined chamber-edifice system for two example volcano sizes (Figures 6 and 7). Overpressure ΔP is set to 100 MPa (except for Figure 7), and $\Delta\rho$ to 300 kg/m^3. Principal deviatoric stresses are evaluated 10 km below the chamber (Figure 2) to determine the capture radius. This allows us to evaluate the relative importance of the surface and the edifice at different depths. For small volcanoes, edifice loading has only a first-order lensing effect for shallow systems (<10 km) with small magma chambers. At a depth of 5 km (Figure 6a), the effect of increasing chamber size is to reduce the capture radius, until

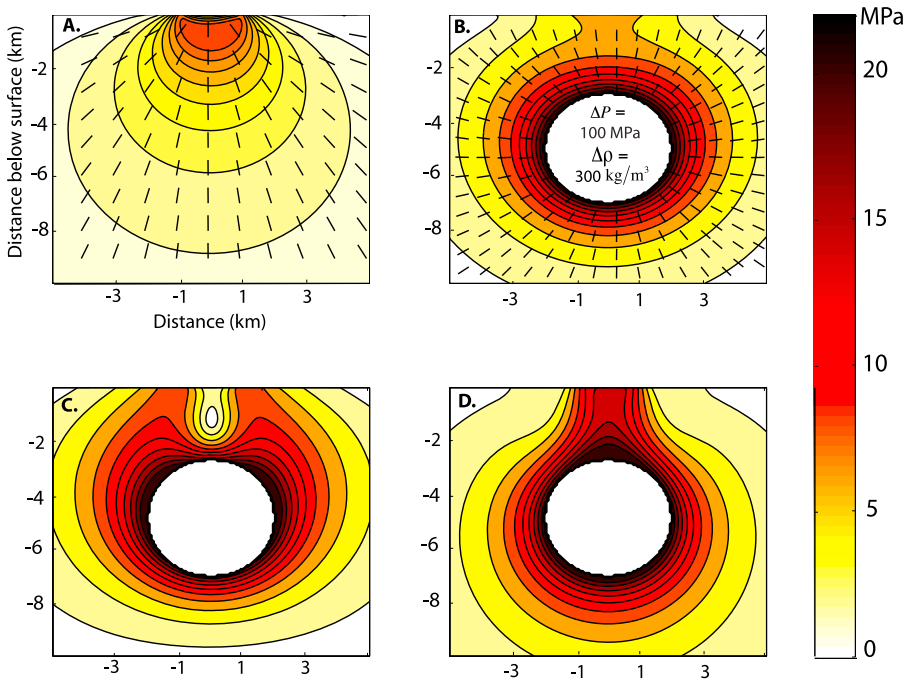

Figure 5. Numerical calculations of tensile deviatoric principal stresses in a 10 km × 10 km area just below the surface. (a) A triangular edifice load with a width of 2 km and height of 1 km on a free surface. Contoured are tensile deviatoric principal stresses (eigenvalues) and selected stress trajectories (eigenvectors) of deviatoric compressional principal stress. (b) A pressurized and buoyant chamber (shaded white for visualization) under a free surface, with no edifice load. Chamber radius is 2 km, depth is 5 km, ΔP = 100 MPa and $\Delta\rho$ = 300 kg/m^3. Contours and stress trajectories are the same as in Figure 5a. (c) Chamber with the edifice of Figure 5a. There is a cancellation of deviatoric stresses above the chamber in this case. (d) Chamber with tensile "edifice" load. Here the stress gradients are in the same direction, resulting in amplified stresses and longer range focusing.

it disappears altogether for chambers of 1 km radius (for the smaller volcanic load). At greater depths, an edifice load acts in a similar way, though with fading influence as chamber depth is increased. The stress cancellation of the combined chamber-edifice system results in a decreased capture radius at depth, although chamber lensing is often the dominant mechanism. In fact, a comparison of the edifice plus chamber system to the chamber alone (Figures 6b–6d) shows that the effect of an edifice on the capture radius 10 km below a chamber becomes negligible at a chamber radius that scales with depth. For these chambers, the edifice is at most a 10% effect. Finally, Figure 6d shows that the free surface ceases to influence chambers deeper than roughly 20 km, and the capture radius approaches that of a chamber in an infinite medium.

[26] The relative size of the volcanic load determines the efficacy of the magma chamber to focus dikes, even if the load alone has no direct influence. This follows from the longer range $1/r$ scaling of stress magnitude with distance from the load. The transition from edifice-dominant to chamber-dominant capture occurs at greater depths, with edifice influence reaching all the way to 20 km depth for small chambers (Figures 6b and 6c). Mechanical interaction between chamber and edifice results in an increase in capture radius over the half-space solution at 10 and 20 km depths for large chambers (>4 km radius), while it decreases the capture radius for smaller chambers.

[27] The effect of magma chamber overpressure is quantified in Figure 7. We choose a particular chamber depth (10 km), and vary chamber overpressure at a fixed radius to find the capture radius 10 km below the chamber (20 km below the free surface). At this depth, only the larger (4 km width) volcano exerts stresses over the 1 MPa threshold. These calculations demonstrate the strongly coupled nature of the combined chamber-edifice loading, and the importance of even small magmatic overpressure. Large chambers (>2 km radius) strongly affect the capture radius, and increasing chamber overpressure results in a transition from edifice-dominated to chamber-dominated lensing. Also plotted are chambers with a smaller (2 km width) volcano, for which only the (albeit rather unrealistic) 4 km radius chamber has a capture radius at this depth (Figure 6b), demonstrating the influence of edifice loading on lensing even when the edifice alone cannot reorient rising melt.

[28] Although we do not treat background stresses explicitly in the present study, regional deviatoric stresses are common in volcanic settings. *Muller et al.* [2001] show that the effect on edifice lensing of a regional deviatoric stress that increases with depth is to decrease the capture radius. We expect a similar effect for chamber lensing. Regional tensile stresses, such as found in extensional tectonic environments such as the Basin and Range may be qualitatively evaluated as similar to the tensile load imposed in Figure 5d. Regional extension will concentrate deviatoric stresses vertically, and hence decrease the capture radius.

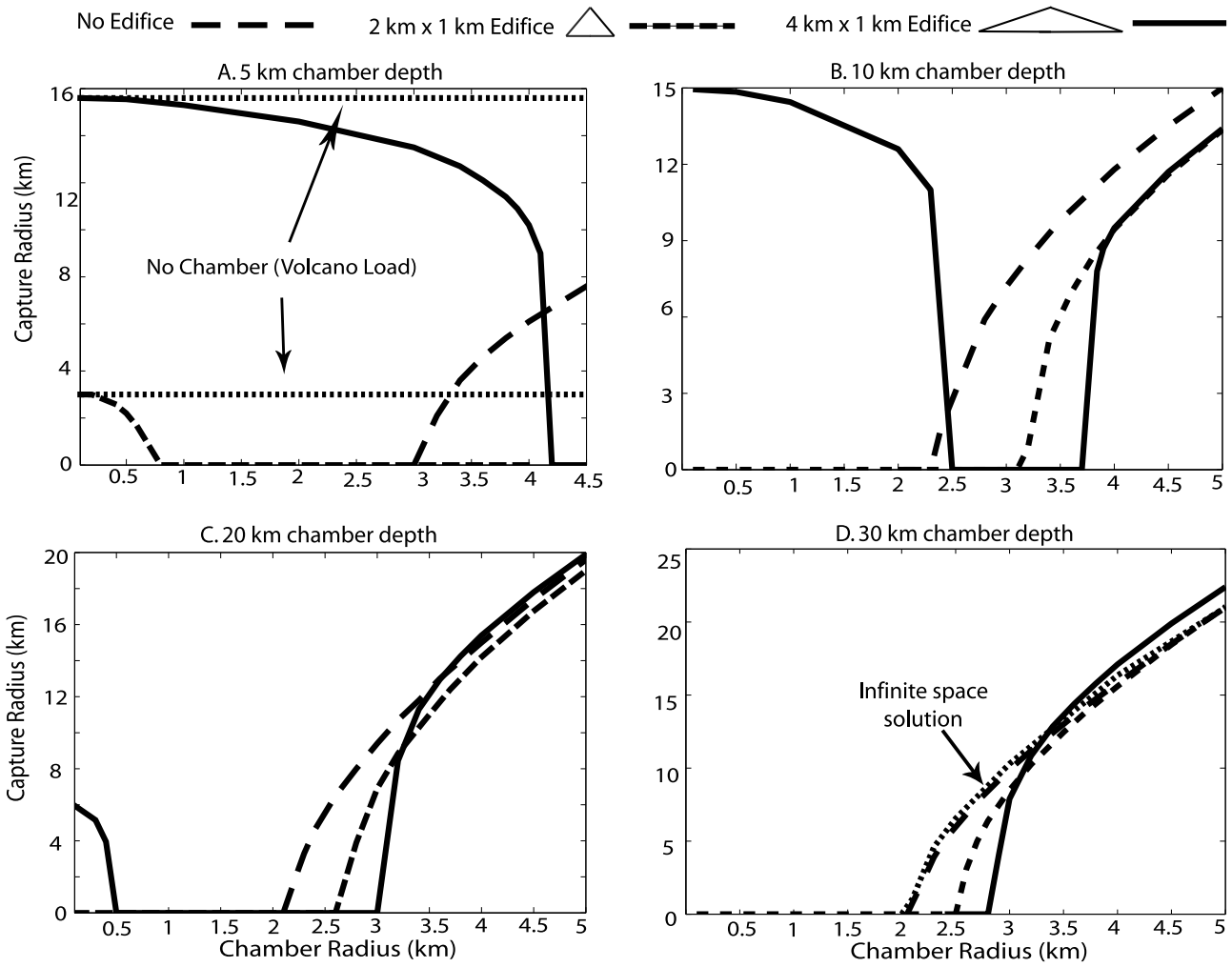

Figure 6. Capture radius of the combined chamber and edifice system, evaluated 10 km below the chamber, at four depths. Chamber overpressure is set to 100 MPa, and buoyancy is set to 300 kg/m^3. Plotted are examples of two volcano sizes (2 km × 1 km and 4 km × 1 km), the half-space solution without an edifice load, and capture radius curves at 15 km depth for edifice loads only, to compare with chamber capture: (a) 5 km chamber depth, (b) 10 km chamber depth, (c) 20 km chamber depth, and (d) 30 km chamber depth.

[29] We treat cylindrical magma chambers in this study, but pressurized magma chambers of more complicated geometries will exhibit stress concentration in regions of high curvature. Seismic observations [e.g., *Barker and Malone*, 1991; *White et al.*, 2008] and geodetic inversions from active volcanic areas [e.g., *Newman et al.*, 2006] suggest ellipsoidal magma chambers at a few kilometers depth, and we expect enhanced lensing (for a given overpressure) in the near field for ellipsoidal chambers of high aspect ratio.

6. Discussion

[30] A magmatic plumbing system is a transport network composed of channels, dikes and magma chambers that, in the case of volcanic centers, drains an area of melt to a discrete point on the surface where it is expressed as a volcano. Except in very special cases (e.g., Hawaii [*Okubo et al.*, 1997]) the subsurface topology and temporal evolution of magmatic plumbing are difficult to observe and are poorly known. There remains considerable debate about the general extent to which intrusive and extrusive igneous processes are connected [e.g., *Bachmann et al.*, 2007], and whether plutonic-scale magma chambers exist at all [e.g., *Glazner et al.*, 2008]. However, even if such large chambers may not necessarily exist at high melt fraction for extended periods of time, the existence of calderas indicates that shallow high melt fraction, extensive, and continuous bodies of magma exist at least transiently. Moreover, long-lived magma storage is often invoked to explain mineral crystallization ages in arc [e.g., *Cooper and Reid*, 2003] and continental [e.g., *Simon and Reid*, 2005] settings, and lower crustal melt accumulation and transport has been documented in a number of arc sections (e.g., Talkeetna [*Hacker et al.*, 2008] and Kohistan [*Jagoutz et al.*, 2007], where concentrically zoned mafic and ultramafic intrusive rocks are suggestive of a large deep chamber). Pressurization, and hence magmatic lensing, should occur whenever an inclusion of ascending melt stalls or accumulates.

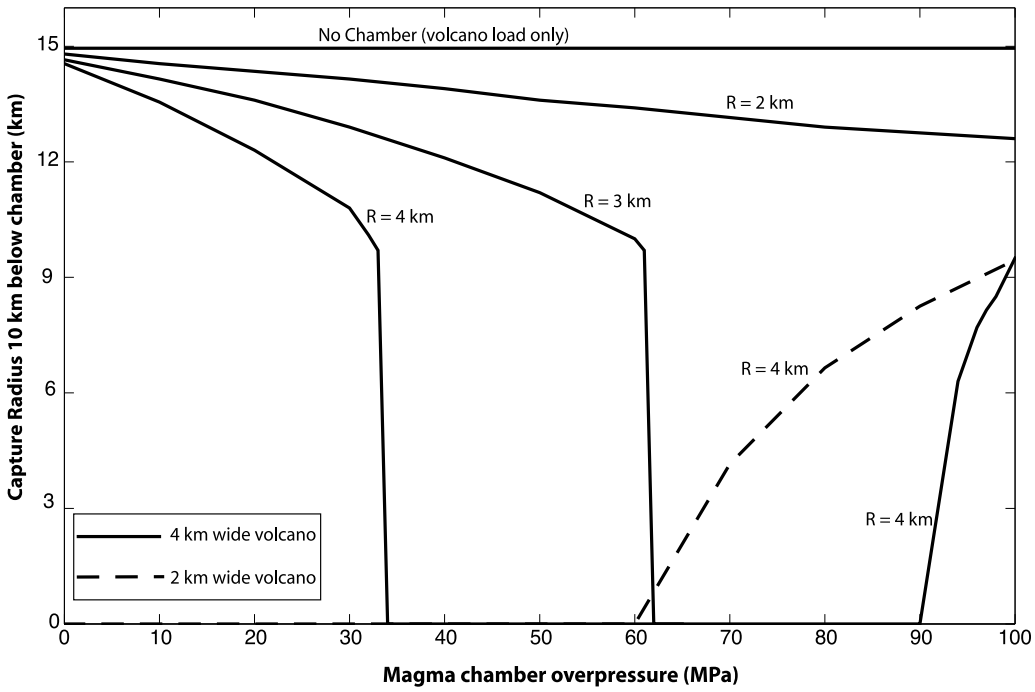

Figure 7. Capture radius of the combined chamber and edifice system 10 km below the chamber, varying magma chamber overpressure. Chamber depth is set to 10 km, and $\Delta\rho$ = 300 kg/m^3. Curves represent chambers of different radii, with two examples of surface volcano loading: a 4 km wide volcano (solid curves) and a 2 km wide volcano (dashed curve). Note from Figure 6b that only 4 km radius chambers have a capture radius at this depth. Plotted for reference is the capture radius of the larger volcano load alone at this depth (25 km below the surface). The smaller load alone does not affect dikes at this depth. The strongly coupled nature of this system is observed for a range of magma chamber overpressure, as is the transition from edifice-dominated to chamber-dominated lensing. Deeper chambers will dominate lensing to a greater degree.

[31] We have shown that dike focusing by components of the plumbing system can be first-order processes and that, while not unique or necessarily mutually exclusive, these effects should be considered viable mechanisms for volcanic center localization. Bottom up models, based on fluid [e.g., *Marsh and Carmichael*, 1974] or elastic [*Vogt*, 1974] instability originating from the melting source region are difficult to test, in part because fundamental aspects of the bottom of the magmatic plumbing system are still poorly understood. A top down perspective is more straightforward to relate to real volcanic systems because the shape and size of volcanic loads are known, and faults can be mapped at the Earth's surface. Previous work has demonstrated that edifice building may affect the volume and compositional evolution of erupted lavas [e.g., *Pinel and Jaupart*, 2000; *Ban and Yamamoto*, 2002] and may affect the trajectories of rising dikes [*Muller et al.*, 2001]. Elastic plate flexure due to edifice loading [e.g., *ten Brink*, 1991; *Hieronymus and Bercovici*, 1999] provides a mechanism for volcano spacing as well as dike focusing, although as noted by *Muller et al.* [2001], it is most effective when the volcano half width is greater than 1/4 times the elastic plate thickness.

[32] However, a solely top-down view of magmatic transport process and organization must still reconcile localization with the need for an initial load. And the presence of calderas whose size dwarfs the preexisting volcanoes [e.g., *Lipman*, 1984] suggests that edifice loading or shallow structural control alone cannot serve to concentrate these prodigious melt bodies. Fluid instability-driven models [e.g., *Marsh and Carmichael*, 1974; *Olson and Singer*, 1985] take the perspective that localization occurs near the magma source region, however this class of models must reconcile a timescale problem relating diapir ascent directly to volcanism, which occurs over a different range of timescales and rheologies [e.g., *Canon-Tapia and Walker*, 2004]. Still, the presence of diapiric melt instabilities cannot be ruled out, and recent tomographic images of the mantle wedge do reveal interesting large-scale upper mantle low seismic velocity structures beneath arc volcanoes in the Japan Trench [*Tamura et al.*, 2002]. Seismic imaging is a promising means of defining active magmatic structures in the crust, and has been successful particularly at shallow (generally < 10 km) depths where it can be corroborated with independent petrologic evidence [e.g., *Auger et al.*, 2001; *Scaillet et al.*, 2008]. Yet deeper magmatic systems remain difficult to observe and interpret [*Lees*, 2007].

[33] We suggest that discrete volcanic centers may also be organized between the source and the surface, through the internal dynamics of magma transport. Several authors have recently begun to explore this possibility, and shown that particular components of a magmatic system (dikes, magma chambers) can coevolve to simultaneously structure and mechanically stabilize the system [e.g., *Ito and Martel*, 2002; *Jellinek and DePaolo*, 2003]. This perspective is in some ways a compromise between the top down and bottom up models, in that features of both fit into the present

framework as end-member cases, but it provides a way for maturing magma plumbing to actively modulate the crustal environment over the lifetime of melt supply.

7. Spacing of Volcanic Centers Around the Pacific Rim

[34] The magmatic lensing mechanism provides a natural length scale for the spacing of volcanic centers: the capture radius of the chamber (Figure 1). However, as demonstrated in Figure 3, the depth at which the capture radius is evaluated (or equivalently, the distance below the chamber from which dikes may be focused) and the depth of the magma chamber beneath the free surface both affect this length scale. As rheological and material interfaces provide a natural location for the formation of large magma chambers [e.g., *Kavanagh et al.*, 2006], we hypothesize that for volcanic systems that develop large magma reservoirs, the spacing of volcanoes may be controlled by the capture radius of a magma chamber at a mid to lower crustal structural discontinuity, such as the Mohorovičić discontinuity (Moho) or the brittle-ductile transition. We compile and analyze a database of volcanoes to test this hypothesis below, noting that there are other plausible alternative hypotheses for chamber depth under arc volcanoes that could be treated in a similar way [e.g., *Pinel and Jaupart*, 2000]. At this stage, we are merely interested in testing whether a simple geometry for arc plumbing systems results in an internally consistent model prediction in the magmatic lensing framework, fully realizing that other localization processes operate in reality.

[35] The spacing of volcanoes on the Earth's surface has been used for decades to compare with models for magmatic plumbing [*Marsh and Carmichael*, 1974; *Vogt*, 1974; *Mohr and Wood*, 1976; *ten Brink*, 1991; *de Bremond d'Ars et al.*, 1995; *Muller et al.*, 2001], but the scatter in spacing is large and it is difficult in many cases to define a single volcanic center from which to base spacing measurements. Indeed, based on this scatter, there exists the opinion that simple measures of volcanic spacing do not support idealized transport theories [e.g., *de Bremond d'Ars et al.*, 1995; *Hildreth*, 2007]. Some studies of volcano spacing try to circumvent the natural variability in volcano spacing by focusing on particular localities, so that regional differences in style and geometry of tectonics might be avoided. However, the continued development of several relevant worldwide geophysical databases provides the opportunity to compare volcanic systems on a global scale, such that it is possible to look for generic features of volcanic processes at increasing levels of detail [e.g., *Hughes and Mahood*, 2008].

[36] We use the volcano database of the Smithsonian Institute's Global Volcanism Program [*Siebert*, 2002], and select stratovolcanoes around the circum-Pacific volcanic belt that clearly correspond to a single center as a proxy for volcanic systems that likely reflect magmatic storage over their lifetimes [e.g., *Cooper and Reid*, 2003]. Because we hypothesize that volcanic plumbing is self-organized in the subsurface, we use only Holocene volcanoes as an estimation of recently active volcanic centers. Stratovolcanoes alone are used in an attempt to include volcanic centers that experience roughly the same dynamic evolution and that may have reasonably long-lived magma chambers. Extinct centers and the extinct volcanoes above them are not considered, but should not contribute significantly to the organization of subsequent systems, provided magma chambers develop beneath the Holocene volcanoes. By hypothesizing the presence of deep storage beneath arc volcanoes, we are assuming that shallow reservoirs do not contribute significantly to volcano spacing; these assumptions define an upper bound on lensing-induced spacing.

[37] We employ stringent criteria for choosing data points within the catalogued volcanoes in the Smithsonian database. We follow the general selection method of *de Bremond d'Ars et al.* [1995], who performed a similar analysis on an earlier version of this database. Details of the selection process are given by *de Bremond d'Ars et al.* [1995], and we provide only a brief summary of our approach. By examining each potential volcanic center, we exclude those that either (1) correspond to the same geographic "center" as another volcano (i.e., are part of the same edifice or edifice complex, which may form after the initial edifice load is established [*Kervyn et al.*, 2009]) or (2) are sufficiently close to other convergent margins that complicated tectonic stresses are likely (i.e., multiple trenches within a few tens of kilometers, or volcanoes that are significant outliers from the trench axis). We do not consider any volcanoes in the South Pacific because of criteria 2, and 27 listed Holocene stratovolcanoes in other locations are excluded by criteria 1 and 2. We included some arc volcanoes not classified as stratovolcanoes (submarine volcanoes in the Mariana Arc [*Fryer*, 1996]). These volcanoes were included to populate our database in areas with thin crust, and each included point was checked to ensure that it is a discrete, recently active volcanic center. This leaves 341 volcanoes in the American Cordillera, Kamchatka, and Japan. Details of all volcanoes, included and excluded, are provided in the auxiliary material.[1] We calculate volcano spacing by finding the spherical arc length between all points in our database with the Haversine Formula. We then run a minimization algorithm to find the nearest neighbor to each volcano. This is an approximation to the more rigorous spacing analysis of *de Bremond d'Ars et al.* [1995], who calculate spacing via a coordinate system local to each arc. We find similar results, and hence do not consider their approach necessary here.

[38] With this spacing data, we use the CRUST 2.0 global crustal model (http://igppweb.ucsd.edu/~gabi/crust2.html) to find the crustal thickness (including sediment) beneath each volcano. The resolution of this model is fairly low at 2×2 degrees, but it is useful nonetheless as it picks out broad-scale regional variability in crustal thickness. The largest model crustal thickness used in this study is 70 km in the Chilean Arc, and the smallest is 6.57 km in the Mariana Arc, encompassing the range of crustal thicknesses found on Earth.

[39] To facilitate visualization of the resulting plot of crustal thickness versus spacing, we bin data points according to crustal thickness, in 10 km bins. Different choices of bin size maintain similar average spacing. The resulting average spacing for each bin along with its standard deviation are shown in Figure 8, along with a histogram

[1] Auxiliary materials are available at ftp://ftp.agu.org/apend/jb/2009JB006339.

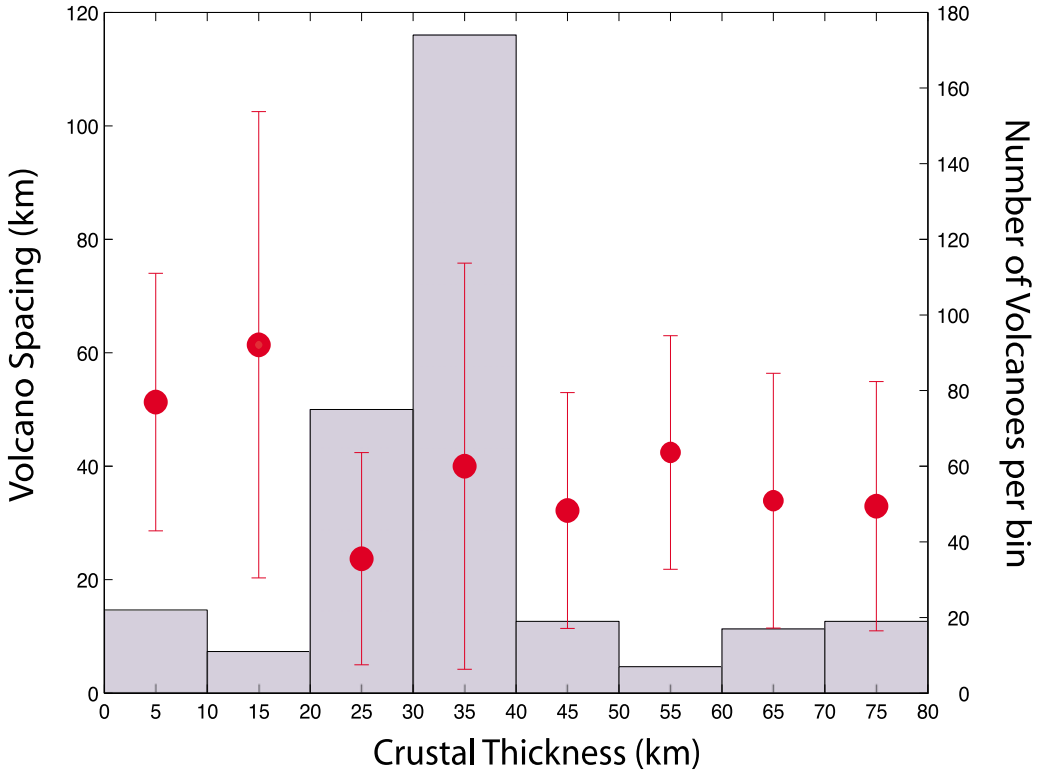

Figure 8. Volcano spacing plotted versus crustal thickness for the circum-Pacific rim volcano database described in the text. Total number of entries is 341. Individual volcano pairs are binned according to crustal thickness (shown in the histogram), then averaged to produce the spacing data points shown. Error bars show one standard deviation. Right-hand scale goes with the histogram, and left-hand scale with the average spacing data. The minimum number of entries in a bin is 9 (50–60 km).

of the data points in each bin. We find that average volcano spacing is 31–43 km in crust thicker than ~20 km and is wider, 56.6 ± 31.7 km, for crustal thicknesses less than ~20 km. It appears, despite the large variance, that there is no significant correlation between crustal thickness and volcano spacing for crust thicker than 20 km, and that for thinner crust there are hints of an anti correlation (Figure 8). Our finding is in contrast to a similar study of volcanoes in the East African Rift Zone [*Mohr and Wood*, 1976] that found a positive correlation between spacing and lithospheric (rather than crustal) thickness. However, we note that *Mohr and Wood* [1976] include data from all Tertiary volcanoes, as well as calderas and other classes of volcanic edifice, which we excluded from our analysis.

[40] These observations, while exhibiting large variability, are generally consistent with our model. Hypothesizing in this case that the primary magma reservoir for arc volcanoes lies at the Moho [e.g., *Kavanagh et al.*, 2006], the parameters that vary most between arcs are the convergence rate, which likely controls melt production rate [e.g., *DeMets et al.*, 1990; *Davies and Bickle*, 1991], and crustal thickness. However, based on other studies [e.g., *de Bremond d'Ars et al.*, 1995] and our own calculations, there is no obvious correlation between plate velocities and arc volcano spacing. Such an observation is consistent with the presence of long-term magma storage in arcs, and that magma transport is heavily modulated subsequent to melt generation. *Muller et al.* [2001] find a rough linear trend between volcano size and spacing in the Cascadia arc, and suggest that this supports top down focusing. We do not discount the possibility that edifice loading affects spacing, but note that edifice size is influenced by eruption volumes and frequency, which may also be related to magma chamber size and magmatic lensing. Additionally, *Muller et al.* [2001] use volcanoes of all types in their analysis, while we restrict ourselves to volcanoes active in the Holocene.

[41] As to the relationship between crustal thickness and volcano spacing, Figure 6 implies that below ~20 km depth, the presence of a free surface (or an edifice load) has a negligible effect on capture radius. This is what we observe in Figure 8, where spacing is largely insensitive to increasing crustal thickness for bins greater than ~20 km. At shallow depths, it is possible that the increase in apparent volcano spacing is a result of discontinuous stress "reflection" from the free surface (Figure 4), and similar arguments would imply a general anti correlation between the depth of magmatic lensing and crustal thickness in arcs. However, a number of complicating factors make this direct comparison more tenuous. As noted by *Fryer* [1996], the distribution of volcanism in the Mariana arc appears to be controlled by faults relating to the processes and geometry of subduction. In such shallow systems, we expect that such features exert dominant control on the organization of the plumbing system. Tectonically induced structural control on shallow features of magmatic systems is likely important in other arcs as well, such as Cascadia [*Hildreth*, 2007]. However, discrete centers are still observed along strike of these faults, and it is possible that focusing due to magma

chambers and volcanic loads operates in conjunction with tectonics to produce the local variability in volcano spacing we observe.

[42] With the understanding, then, that our or any idealized model cannot hope to capture the variability in Figure 8, we are nonetheless interested in calculating the spacing implied by the magma lensing model (with no edifice load). Model predictions that fit the observational data are nonunique, as there is a trade-off between chamber size and overpressure for a given result. To produce a capture radius of ~15–20 km at depths greater than ~20 km, a 1.5 km radius magma chamber at the Moho would need to have 100 MPa of overpressure, while a 4 km radius chamber needs 20 MPa. Our observations and calculations are thus self-consistent, resulting in a reasonable range of values for both chamber radius and overpressure to produce the observed mean volcano spacing.

8. Conclusion

[43] As has been recognized in both field-based and statistical studies of volcano spacing in arcs, there is little support for the idealized view of arc volcanoes as single or double chains of evenly spaced edifices. However, the existence and distribution of volcanoes as primary surface expressions of terrestrial magmatism requires explanation. Our calculations suggest a mechanism by which magma chambers can organize and modulate transport processes within the crust. This magmatic lensing should be considered an extension of the proposed focusing of rising dikes by volcanic edifices, and it is an independently operating mechanism within the initial confines of local structures and tectonics; we have shown that magma chamber lensing of dikes is more effective than edifice lensing in many cases. While the maximum capture radius of an edifice alone (in an isotropic background stress field) is on the order of 10–20 times the edifice size [*Muller et al.*, 2001], the capture radius of a magma chamber alone is greater or equal in magnitude for realistic chamber overpressures. Shallow magma chambers and long-lived, high-volume reservoirs should dominate mechanical organization of the system. Further, we have shown that the combined stresses of a chamber and an edifice are strongly coupled, and that in fact the presence of an edifice acts to reduce the capture radius of the system when the dimensions of the chamber and edifice are the same order of magnitude.

[44] It has been suggested [e.g., *Pinel and Jaupart*, 2000] that these coupled systems form due to edifice loading, which creates a density trap at shallow depths below the edifice. Such chambers do not resolve the question of initial volcanic center discretization, but may provide a stabilizing feedback to the spacing of the system once it is established. Discrete magmatic centers may form before a volcanic edifice is built, however, if a deeper chamber forms prior to the first surface eruption. It seems plausible that in fact multiple chambers exist within a given plumbing system, set by the various rheological boundaries and structures that exist between the source region and the surface, stabilized by the internal lensing dynamics. The apparent dichotomy between small closely spaced centers and larger widely spaced edifices that has been observed in some arcs (e.g., Cascadia [*Hildreth*, 2007] and the Central Andes [*Savant and de Silva*, 2005]) may in this light reflect the interaction of tectonics and magmatic lensing at different levels within the crust.

[45] Systems that operate via magmatic lensing, particularly if multilevel magma storage occurs, should sample magmas of potentially diverse composition. These chambers could then function as places of magma homogenization similar to the proposed MASH zones of the lower crust [e.g., *Hildreth and Moorbath*, 1988]. Erupted lavas in these systems would then represent the integrated hybridized upwelling magmatic signal from a broad region of the crust.

[46] Magma chambers need not be present under all volcanoes, especially sites (often associated with oceanic islands) that more directly sample primitive magmas, and in these environments it may be that surface loading controls the focusing of rising magma into discrete centers [*Hieronymus and Bercovici*, 1999]. But a broad array of volcanological settings do require magma storage prior to eruption, and in these cases we suggest that magma chambers play an organizational role in the formation of volcanic centers. The subsequent longevity and stability of the center may also be governed by magma chamber dynamics [*Jellinek and DePaolo*, 2003] resulting from the combined interaction of thermally induced rheological evolution of the country rock, melt supply, and chamber depth (Karlstrom et al., submitted manuscript, 2009), which in turn depend on tectonic environment.

[47] Finally, we note that pressurized dikes exhibit a focusing behavior similar to the magma chambers presented here [*Ito and Martel*, 2002; *O'Neill et al.*, 2007] and so may be expected to play a role in developing plumbing systems. However, despite a range of interesting dike interactions [*Ito and Martel*, 2002], in the presence of a larger background stress (such as a large magma chamber or volcano), these effects will be heavily damped. Dike interactions, and the smaller-scale stress-induced reorientation of channelized melt, may be most important where far-field loads are not present, and may be responsible for the creation of sizable magma chambers.

[48] Lensing of rising melt by the components of a magmatic plumbing system such as dikes, chambers and volcanic edifices is a concise theoretical framework for understanding active localization of volcanic activity on Earth's surface. The structure of the plumbing system, and which of the above dominates lensing, should depend on tectonic environment, structural controls and magma supply rate, and hence vary from place to place. It is likely that edifice morphology, lava composition, and erupted volumes are also a strong function of the subsurface topology; a better characterization of these plumbing systems is certainly warranted to further explore this possibility. However, we suggest that magmatic lensing plays an important role in the set of processes that govern volcanic plumbing, and provides a mechanism that, once established, may evolve to modulate structural anisotropy and inhomogeneity in the crust. In this way, it provides a means of affecting regional tectonics and sustaining long-lived, multilevel magmatic systems.

Appendix A

[49] Solutions to the equations of linear elasticity in two dimensions may be found by the method of stress functions

[*Fung*, 1965] whereby the equilibrium equations are satisfied by a scalar function χ satisfying the biharmonic equation:

$$\nabla^4 \chi = 0 \tag{A1}$$

and the appropriate boundary conditions. With this function stresses, in a two dimensional orthogonal coordinate system in which the coefficients of the metric are equal, are given by

$$\sigma_{11} = h\frac{\partial}{\partial q_2}\left(h\frac{\partial \chi}{\partial q_2}\right) - h\frac{\partial h}{\partial q_1}\frac{\partial \chi}{\partial q_1} \tag{A2}$$

$$\sigma_{22} = h\frac{\partial}{\partial q_1}\left(h\frac{\partial \chi}{\partial q_1}\right) - h\frac{\partial h}{\partial q_2}\frac{\partial \chi}{\partial q_2} \tag{A3}$$

$$\sigma_{12} = -h\frac{\partial^2 (h\chi)}{\partial q_1 \partial q_2} + h\chi\frac{\partial^2 h}{\partial q_1 \partial q_2} \tag{A4}$$

where q_1 and q_2 are spatial coordinates, and h is the coefficient of the metric [*Love*, 1944].

[50] We use the bipolar coordinate system, given in terms of cartesian coordinates by the complex mapping [e.g., *Jeffery*, 1921; *Pinel and Jaupart*, 2000]

$$x + iy = \frac{k(\sinh\alpha + i\sin\beta)}{\cosh\alpha - \cos\beta} \tag{A5}$$

Here α and β are spatial coordinates; curves of constant α and β trace orthogonally intersecting circles, $i = \sqrt{-1}$, and k is a dimensional constant equal to one half the distance between the two foci of the coordinate system, curves of constant α [*Jeffery*, 1921]. In this coordinate system, the problem of a circular cavity in a half-space is naturally posed: the cavity and the free surface are given by $\alpha = \alpha_0$ and $\alpha = 0$. The radius of the cavity is then

$$R = k\ \mathrm{csch}(\alpha_0) \tag{A6}$$

and the straight-line distance from the free surface to the center of the cavity is

$$d = k\tanh(\alpha_0/2) \tag{A7}$$

Boundary conditions (equations (1)–(4)) are now given by

$$\begin{aligned}\sigma_{\alpha\alpha}|_{\alpha=\alpha_0} &= \Delta P + \Delta\rho g y \\ &= \Delta P + \Delta\rho g k\left(1 + 2\sum_{n=1}^{\infty} e^{-n\alpha_0}\cos(n\beta)\right)\end{aligned} \tag{A8}$$

$$\sigma_{\alpha\beta}|_{\alpha=\alpha_0} = \sigma_{\alpha\alpha}|_{\alpha=0} = \sigma_{\alpha\beta}|_{\alpha=0} = 0 \tag{A9}$$

[51] Stress functions that satisfy equation (A1) and these boundary conditions take the general form

$$\chi = \sum_{n=0}^{\infty} f_n(\alpha)\cos(n\beta) \tag{A10}$$

We find that a three term expansion of this sum captures the details; the contribution of higher-order terms is small. Therefore, we use the following approximate stress function:

$$\begin{aligned}\chi =& A_1\alpha k + \frac{1}{h}(B_1(\cosh(2\alpha) - 1) + C_1\sinh(2\alpha))\cos(\beta) \\ &+ \frac{1}{h}(A_2(\cosh(3\alpha) - \cosh(\alpha)) + B_2(\sinh(3\alpha) - 3\sinh(\alpha)) \\ &\cdot \cos(2\beta))\end{aligned} \tag{A11}$$

where $h = k^{-1}(\cosh\alpha - \cos\beta)$ and the A_n and B_n are constants evaluated to satisfy the boundary conditions. After doing so, the final stress components are

$$\begin{aligned}\sigma_{\alpha\alpha}(\alpha,\beta) =& e^{-3\alpha_0}\left(\frac{\sinh(\alpha)}{\sinh(\alpha_0)}\right)^2\{e^{3\alpha_0}(\Delta P + k\Delta\rho g) + \mathrm{csch}(\alpha_0) \\ &\cdot [-k\Delta\rho g\cos(3\beta)\cdot(\cosh(\alpha) - \cosh(\alpha - 2\alpha_0) \\ &+ \sinh(\alpha) + 7\sinh(\alpha - 2\alpha_0)) + k\Delta\rho g\cos(2\beta) \\ &\cdot (2 + 3\cosh(2\alpha) - 3\cosh(2(\alpha - \alpha_0)) \\ &- 2\cosh(2\alpha_0) + 15\sinh(2\alpha_0) + 21\sinh(2(\alpha - \alpha_0)) \\ &- 14\sinh(2\alpha_0)) - e^{\alpha_0}\cos(\beta)\cdot[(\Delta P + 10k\Delta\rho g) \\ &\cdot \cosh(\alpha - 3\alpha_0) + k\Delta\rho g(\cosh(\alpha - \alpha_0) \\ &- 11\cosh(\alpha + \alpha_0) + 30\cosh(\alpha_0)\sinh(\alpha) \\ &+ 8(\sinh(\alpha - 3\alpha_0) - 2\cosh(\alpha)\sinh(\alpha_0))) \\ &- \Delta P(\cosh(\alpha - 3\alpha_0) + \sinh(\alpha - 3\alpha_0) \\ &+ \sinh(\alpha + \alpha_0))]]\},\end{aligned} \tag{A12}$$

$$\begin{aligned}\sigma_{\beta\beta}(\alpha,\beta) =& \frac{1}{4}e^{-3\alpha_0}\mathrm{csch}^2(\alpha_0)\{-2e^{3\alpha_0}(\Delta P + k\Delta\rho g) \\ &\cdot (1 + \cosh(2\alpha)) + 2e^{-2(\alpha+\alpha_0)}(-9e^{2\alpha_0}k\Delta\rho g \\ &- 11e^{4\alpha_0}k\Delta\rho g + e^{6\alpha_0}(\Delta P + k\Delta\rho g) \\ &+ e^{2\alpha}\left(-1 + e^{2\alpha_0}\right)\left(k\Delta\rho g\left(3 + 4e^{2\alpha_0} + e^{4\alpha_0}\right)\right. \\ &\left.+ \Delta P e^{4\alpha_0}\right) + e^{4\alpha}(k\Delta\rho g(9 + 12e^{(2\alpha_0)} - 2e^{4\alpha_0}) \\ &+ \Delta P e^{4\alpha_0}))\cos(\beta)\left(\frac{\cosh(\alpha)}{\sinh(\alpha_0)}\right) - e^{-2(2\alpha+\alpha_0)} \\ &\cdot \cos(2\beta)\mathrm{csch}(\alpha_0)(e^{2\alpha_0}(-6 - 18e^{2\alpha} - e^{4\alpha} \\ &+ 24e^{6\alpha} + 9e^{8\alpha})k\Delta\rho g + 2e^{2\alpha+6\alpha_0}(\Delta P + 2k\Delta\rho g) \\ &- 2e^{4\alpha_0}\left(k\Delta\rho g\left(6 + 11e^{2\alpha} - 2e^{4\alpha} + 2e^{6\alpha}\right) + e^{6\alpha}\Delta P\right) \\ &+ 6e^{6\alpha}k\Delta\rho g(3 + \cosh(2\alpha) + 2\sinh(2\alpha))) \\ &- k\Delta\rho g\cos(3\beta)\mathrm{csch}(\alpha_0)[\cosh(\alpha + 2\alpha_0) \\ &+ 15\sinh(\alpha) - 25\sinh(3\alpha) + 7(2\sinh(\alpha - 2\alpha_0) \\ &- 5\sinh(3\alpha - 2\alpha_0) + \sinh(\alpha + 2\alpha_0))]\},\end{aligned} \tag{A13}$$

$$\begin{aligned}\sigma_{\alpha\beta}(\alpha,\beta) =& -\frac{1}{2}e^{-7\alpha_0}\left(1 + e^{4\alpha_0}\right)(\cos(\beta) - \cosh(\alpha))\mathrm{csch}^3(\alpha_0) \\ &\cdot \mathrm{sech}(2\alpha_0)\sin(\beta)\cdot\sinh(\alpha)\{e^{-\alpha+6\alpha_0}(\Delta P + k\Delta\rho g) \\ &- 6\left(1 + 3e^{2\alpha}\right)k\Delta\rho g\cos(\beta) - e^{4\alpha_0} \\ &\cdot [k\Delta\rho g(-32\cos(\beta)\cosh^2(\alpha) + \sinh(\alpha) \\ &\cdot (3 - 16\cos(\beta)\sinh(\alpha)) + \sinh(\alpha)\Delta P) \\ &+ \cosh(\alpha)(\Delta P + k\Delta\rho g(1 + 48\cos(\beta)\sinh(\alpha)))] \\ &- 2e^{2\alpha_0}k\Delta\rho g[\cos(\beta) - 3\sinh(\alpha) + 3\cos(\beta) \\ &\cdot (\cosh(2\alpha) + 5\sinh(2\alpha))]\}\end{aligned} \tag{A14}$$

Deviatoric stresses, from which the conclusions in the text are based, follow from the tensor equation

$$\sigma^{dev} = \sigma - \mathrm{tr}(\sigma) \tag{A15}$$

and principal stresses are eigenvalues of the corresponding component matrix.

[52] **Acknowledgments.** The presentation and scope of our work improved considerably after detailed comments by two anonymous reviewers. This research was funded by NSF EAR0608885 and NASA 08-MFRP08-0073 grants to M.M.

References

Anderson, E. M. (1951), *The Dynamics of Faulting and Dyke Formation With Applications to Britain*, Oliver and Boyd, White Plains, N. Y.

Annen, C., and R. S. J. Sparks (2002), Effects of repetitive emplacement of basaltic intrusions on thermal evolution and melt generation in the crust, *Earth Planet. Sci. Lett.*, *203*, 937–955, doi:10.1016/S0012-821X(02)00929-9.

Atkinson, B. K., and P. G. Meredith (1987), The theory of subcritical crack growth with application to minerals and rocks, in *Fracture Mechanics of Rock*, edited by B. K. Atkinson, pp. 111–166, Academic, New York.

Auger, E., P. Gasparini, J. Virieux, and A. Zollo (2001), Seismic evidence of an extended magmatic sill under Mt. Vesuvius, *Science*, *294*, 1510–1512, doi:10.1126/science.1064893.

Bachmann, O., C. Miller, and S. de Silva (2007), The volcanic-plutonic connection as a stage for understanding crustal magmatism, *J. Volcanol. Geotherm. Res.*, *167*, 1–23, doi:10.1016/j.jvolgeores.2007.08.002.

Ban, M., and T. Yamamoto (2002), Petrological study of Nasu-Chausudake volcano (ca. 16 ka to present) northeastern Japan, *Bull. Volcanol.*, *64*, 100–116, doi:10.1007/s00445-001-0187-9.

Barker, S. E., and S. D. Malone (1991), Magmatic system geometry at Mount St. Helens modeled from the stress field associated with posteruptive earthquakes, *J. Geophys. Res.*, *96*(B7), 11,883–11,894, doi:10.1029/91JB00430.

Canon-Tapia, E., and G. P. Walker (2004), Global aspects of volcanism: The perspectives of "plate tectonics" and "volcanic systems," *Earth Sci. Rev.*, *66*, 163–182, doi:10.1016/j.earscirev.2003.11.001.

Chen, Z., and Z.-H. Jin (2006), Magma-driven subcritical crack growth and implications for dike initiation from a magma chamber, *Geophys. Res. Lett.*, *33*, L19307, doi:10.1029/2006GL026979.

Cooper, K. M., and M. R. Reid (2003), Re-examination of crystal ages in recent Mount St. Helens lavas: implications for magma reservoir processes, *Earth Planet. Sci. Lett.*, *213*, 149–167, doi:10.1016/S0012-821X(03)00262-0.

Davies, J. H., and M. J. Bickle (1991), A physical model for the volume and composition of melt produced by hydrous fluxing above subduction zones, *Philos. Trans. R. Soc. London A*, *335*, 355–364, doi:10.1098/rsta.1991.0051.

de Bremond d'Ars, J., C. Jaupart, and R. S. J. Sparks (1995), Distribution of volcanoes in active margins, *J. Geophys. Res.*, *100*(B10), 20,421–20,432, doi:10.1029/95JB02153.

DeMets, C., R. G. Gordon, D. F. Argus, and S. Stein (1990), Current plate motions, *Geophys. J. Int.*, *101*, 425–478, doi:10.1111/j.1365-246X.1990.tb06579.x.

de Silva, S. L., and W. D. Gosnold (2007), Episodic construction of batholiths: Insights from the spatiotemporal development of an ignimbrite flare-up, *J. Volcanol. Geotherm. Res.*, *167*, 320–335, doi:10.1016/j.jvolgeores.2007.07.015.

Dimalanta, C., A. Taira, G. P. J. Yumul, H. Tokuyama, and K. Mochizuki (2002), New rates of western Pacific island arc magmatism from seismic and gravity data, *Earth Planet. Sci. Lett.*, *202*, 105–115, doi:10.1016/S0012-821X(02)00761-6.

Dragoni, M., and C. Magnanensi (1989), Displacement and stress produced by a pressurized, spherical magma chamber, surrounded by a viscoelastic shell, *Phys. Earth Planet. Inter.*, *56*, 316–328, doi:10.1016/0031-9201(89)90166-0.

Dufek, J., and G. W. Bergantz (2005), Lower crustal magma genesis and preservation: A stochastic framework for the evaluation of basalt-crust interaction, *J. Petrol.*, *46*(11), 2167–2195, doi:10.1093/petrology/egi049.

Dumond, G., K. H. Mahan, M. L. Williams, and K. E. Karlstrom (2007), Crustal segmentation, composite looping pressure-temperature paths, and magma-enhanced metamorphic field gradients: Upper Granite Gorge, Grand Canyon, USA, *Geol. Soc. Am. Bull.*, *119*(1), 202–220, doi:10.1130/B25903.1.

Folch, A., and J. Marti (1998), The generation of overpressure in felsic magma chambers by replenishment, *Earth Planet. Sci. Lett.*, *163*, 301–314, doi:10.1016/S0012-821X(98)00196-4.

Fryer, P. (1996), Evolution of the mariana convergent plate margin system, *Rev. Geophys.*, *34*(1), 89–125, doi:10.1029/95RG03476.

Fung, Y. C. (1965), *Foundations of Solid Mechanics*, Prentice-Hall, Englewood Cliffs, N. J.

Galland, O., P. R. Cobbold, J. de Bremond d'Ars, and E. Hallot (2007), Rise and emplacement of magma during horizontal shortening of the brittle crust: Insights from experimental modeling, *J. Geophys. Res.*, *112*, B06402, doi:10.1029/2006JB004604.

Gao, X.-W., and T. G. Davies (2002), *Boundary Element Programming in Mechanics*, Cambridge Univ. Press, Cambridge, U. K.

Glazner, A. F., D. S. Coleman, and J. M. Bartley (2008), The tenuous connection between high-silica rhyolites and granodiorite plutons, *Geology*, *36*(2), 183–186, doi:10.1130/G24496A.1.

Griffith, A. A. (1920), The phenomena of rupture and flow in solids, *Philos. Trans. R. Soc. London*, *221*, 163–197.

Grosfils, E. B. (2007), Magma reservoir failure on the Terrestrial planets: Assessing the importance of gravitational loading in simple elastic models, *J. Volcanol. Geotherm. Res.*, *166*, 47–75, doi:10.1016/j.jvolgeores.2007.06.007.

Gudmundsson, A. (1988), Effect of tensile stress concentration around magma chambers on intrusion and extrusion frequencies, *J. Volcanol. Geotherm. Res.*, *35*, 179–194, doi:10.1016/0377-0273(88)90015-7.

Gudmundsson, A. (2006), How local stresses control magma-chamber ruptures, dyke injections, and eruptions in composite volcanoes, *Earth Sci. Rev.*, *79*, 1–31, doi:10.1016/j.earscirev.2006.06.006.

Hacker, B. R., L. Mehl, P. B. Kelemen, M. Rioux, M. D. Behn, and P. Luffi (2008), Reconstruction of the Talkeetna intraoceanic arc of Alaska through thermobarometry, *J. Geophys. Res.*, *113*, B03204, doi:10.1029/2007JB005208.

Hieronymus, C. F., and D. Bercovici (1999), Discrete alternating hotspot islands formed by interaction of magma transport and lithospheric flexure, *Nature*, *397*, 604–607, doi:10.1038/17584.

Hildreth, W. (2007), Quaternary magmatism in the Cascades-Geologic perspectives, *U.S. Geol. Surv. Prof., 1744*.

Hildreth, W., and S. Moorbath (1988), Crustal contributions to arc magmatism in the Andes of central Chile, *Contrib. Mineral. Petrol.*, *98*, 455–489, doi:10.1007/BF00372365.

Hughes, G. R., and G. A. Mahood (2008), Tectonic controls on the nature of large silicic calderas in volcanic arcs, *Geology*, *36*(8), 627–630, doi:10.1130/G24796A.1.

Ihinger, P. D. (1995), Mantle flow beneath the Pacific plate-Evidence from seamount segments in the Hawaiian-Emperor chain, *Am. J. Sci.*, *295*(9), 1035–1057.

Ito, G., and S. J. Martel (2002), Focusing of magma in the upper mantle through dike interaction, *J. Geophys. Res.*, *107*(B10), 2223, doi:10.1029/2001JB000251.

Jagoutz, O., O. Muntener, P. Ulmer, T. Pettke, and J. Burg (2007), Petrology and mineral chemistry of lower crust intrusions: The Chilas complex, Kohistan (NW Pakistan), *J. Petrol.*, *48*(10), 1895–1953, doi:10.1093/petrology/egm044.

Jeffery, G. B. (1921), Plain stress and plane strain in bipolar co-ordinates, *Philos. Trans. R. Soc. London A*, *221*, 265–293, doi:10.1098/rsta.1921.0009.

Jellinek, A. M., and D. J. DePaolo (2003), A model for the origin of large silicic magma chambers: precursors of caldera-forming eruptions, *Bull. Volcanol.*, *65*, 363–381, doi:10.1007/s00445-003-0277-y.

Kavanagh, J. L., T. Menand, and R. S. J. Sparks (2006), An experimental investigation of sill formation and propagation in layered elastic media, *Earth Planet. Sci. Lett.*, *245*, 799–813, doi:10.1016/j.epsl.2006.03.025.

Kervyn, M., G. G. J. Ernst, B. van Wyk de Vries, L. Mathieu, and P. Jacobs (2009), Volcano load control on dyke propagation and vent distribution: Insights from analogue modeling, *J. Geophys. Res.*, *114*, B03401, doi:10.1029/2008JB005653.

Lees, J. M. (2007), Seismic tomography of magmatic systems, *J. Volcanol. Geotherm. Res.*, *167*, 37–56, doi:10.1016/j.jvolgeores.2007.06.008.

Lipman, P. W. (1984), The roots of ash flow calderas in western North America: Windows into the tops of granitic batholiths, *J. Geophys. Res.*, *89*(B10), 8801–8841, doi:10.1029/JB089iB10p08801.

Love, A. E. H. (1944), *Treatise on the Mathematical Theory of Elasticity*, Dover, New York.

Marsh, B. D., and I. S. Carmichael (1974), Benioff-zone magmatism, *J. Geophys. Res.*, *79*(8), 1196–1206, doi:10.1029/JB079i008p01196.

Massonnet, D., P. Briole, and A. Arnaud (1995), Deflation of Mount Etna monitored by spaceborne radar interferometry, *Nature*, *375*, 567–570, doi:10.1038/375567a0.

Mériaux, C., and J. R. Lister (2002), Calculation of dike trajectories from volcanic centers, *J. Geophys. Res.*, *107*(B4), 2077, doi:10.1029/2001JB000436.

Mohr, P. A., and C. A. Wood (1976), Volcano spacings and lithospheric attenuation in the eastern rift of Africa, *Earth Planet. Sci. Lett.*, *33*, 126–144, doi:10.1016/0012-821X(76)90166-7.

Muller, J. R., G. Ito, and S. J. Martel (2001), Effects of volcano loading on dike propagation in an elastic half-space, *J. Geophys. Res.*, *106*(B6), 11,101–11,113, doi:10.1029/2000JB900461.

Nakamura, K., K. H. Jacob, and J. N. Davies (1977), Volcanoes as possible indicators of tectonic stress orientation—Aleutians and Alaska, *Pure Appl. Geophys.*, *115*(1–2), 87–112, doi:10.1007/BF01637099.

Newman, A. V., T. H. Dixon, G. I. Ofoegbu, and J. E. Dixon (2001), Geodetic and seismic constraints on recent activity at Long Valley Caldera, California: Evidence for viscoelastic rheology, *J. Volcanol. Geotherm. Res.*, *105*, 183–206, doi:10.1016/S0377-0273(00)00255-9.

Newman, A. V., T. H. Dixon, and N. Gourmelen (2006), A four-dimensional viscoelastic deformation model for Long Valley caldera, California, between 1995 and 2000, *J. Volcanol. Geotherm. Res.*, *150*, 244–269, doi:10.1016/j.jvolgeores.2005.07.017.

Odé, H. (1957), Mechanical analysis of the dike pattern of the Spanish Peaks area, Colorado, *Geol. Soc. Am. Bull.*, *68*, 567–576, doi:10.1130/0016-7606(1957)68[567:MAOTDP]2.0.CO;2.

Okubo, P. G., H. M. Benz, and B. A. Chouet (1997), Imaging the crustal magma sources beneath Mauna Loa and Kilauea volcanoes, Hawaii, *Geology*, *25*(10), 867–870, doi:10.1130/0091-7613(1997)025<0867:ITCMSB>2.3.CO;2.

Olson, P., and H. Singer (1985), Creeping plumes, *J. Fluid Mech.*, *158*, 511–531, doi:10.1017/S0022112085002749.

O'Neill, C., A. Lenardic, A. M. Jellinek, and W. S. Kiefer (2007), Melt propagation and volcanism in mantle convection simulations, with applications for Martian volcanic and atmospheric evolution, *J. Geophys. Res.*, *112*, E07003, doi:10.1029/2006JE002799.

Petcovic, H. L., and J. Dufek (2005), Modeling magma flow and cooling in dikes: Implications for emplacement of Columbia River flood basalts, *J. Geophys. Res.*, *110*, B10201, doi:10.1029/2004JB003432.

Pinel, V., and C. Jaupart (2000), The effect of edifice load on magma ascent beneath a volcano, *Philos. Trans. R. Soc. London A*, *358*, 1515–1532, doi:10.1098/rsta.2000.0601.

Pinel, V., and C. Jaupart (2003), Magma chamber behavior beneath a volcanic edifice, *J. Geophys. Res.*, *108*(B2), 2072, doi:10.1029/2002JB001751.

Pritchard, M. E., and M. Simons (2004), An InSAR-based survey of volcanic deformation in the central Andes, *Geochem. Geophys. Geosyst.*, *5*, Q02002, doi:10.1029/2003GC000610.

Rapp, R. P., and E. B. Watson (1995), Dehydration melting of metabasalt at 8–32 kbar: Implications for continental growth and crust-mantle recycling, *J. Petrol.*, *36*(4), 891–931.

Rubin, A. M. (1995a), Getting granite dikes out of the source region, *J. Geophys. Res.*, *100*(B4), 5911–5929, doi:10.1029/94JB02942.

Rubin, A. M. (1995b), Propagation of magma-filled cracks, *Annu. Rev. Earth Planet. Sci.*, *23*, 287–336, doi:10.1146/annurev.ea.23.050195.001443.

Sartoris, G., J. P. Pozzi, C. Phillippe, and J. L. L. Mouel (1990), Mechanical stability of shallow magma chambers, *J. Geophys. Res.*, *95*(B4), 5141–5151, doi:10.1029/JB095iB04p05141.

Savant, S. S., and S. L. de Silva (2005), A GIS-based spatial analysis of volcanoes in the Central Andes: Insights into factors controlling volcano spacing, *Eos Trans. AGU*, *86*(52), Fall Meeting Suppl., Abstract V21D-0648.

Scaillet, B., M. Pichavant, and R. Cioni (2008), Upward migration of Vesuvius magma chamber over the past 20,000 years, *Nature*, *455*, 216–219, doi:10.1038/nature07232.

Siebert, S. T. (2002), Volcanoes of the world: An illustrated catalog of Holocene volcanoes and their eruptions, Global Volcanism Program Digital Inf. Ser. GVP-3, Smithson. Inst., Washington, D. C. (Available at http://www.volcano.si.edu/world)

Simon, J. I., and M. R. Reid (2005), The pace of rhyolite differentiation and storage in an 'archetypical' silicic magma system, Long Valley, California, *Earth Planet. Sci. Lett.*, *235*, 123–140, doi:10.1016/j.epsl.2005.03.013.

Spiegelman, M. (1993), Flow in deformable porous media. Part 1: Simple analysis, *J. Fluid Mech.*, *247*, 17–38, doi:10.1017/S0022112093000369.

Stasuik, M. V., C. Jaupart, and R. S. J. Sparks (1993), On the variation of lava flow rate in non-explosive lava eruptions, *Earth Planet. Sci. Lett.*, *114*, 505–516, doi:10.1016/0012-821X(93)90079-O.

Tait, S., C. Jaupart, and S. Vergniolle (1989), Pressure, gas content and eruption periodicity of a shallow, crystallizing magma chamber, *Earth Planet. Sci. Lett.*, *92*, 107–123, doi:10.1016/0012-821X(89)90025-3.

Tamura, Y., Y. Tatsumi, D. Zhao, Y. Kido, and H. Shukuno (2002), Hot fingers in the mantle wedge: new insights into magma genesis in subduction zones, *Earth Planet. Sci. Lett.*, *197*, 105–116, doi:10.1016/S0012-821X(02)00465-X.

ten Brink, U. (1991), Volcano spacing and plate rigidity, *Geology*, *19*, 397–400, doi:10.1130/0091-7613(1991)019<0397:VSAPR>2.3.CO;2.

Vigneresse, J.-L., B. Tikoff, and L. Ameglio (1999), Modification of the regional stress field by magma intrusion and formation of tabular granitic plutons, *Tectonophysics*, *302*, 203–224, doi:10.1016/S0040-1951(98)00285-6.

Vogt, P. R. (1974), Volcano spacing, fractures, and thickness of the lithosphere, *Earth Planet. Sci. Lett.*, *21*, 235–252, doi:10.1016/0012-821X(74)90159-9.

White, R. S., et al. (2008), Lower-crustal intrusion on the North Atlantic continental margin, *Nature*, *452*, 460–464, doi:10.1038/nature06687.

Yun, S., P. Segall, and H. Zebker (2006), Constraints on magma chamber geometry at Sierra Negra volcano, Galapagos Islands, based on InSAR observations, *J. Volcanol. Geotherm. Res.*, *150*, 232–243, doi:10.1016/j.jvolgeores.2005.07.009.

J. Dufek, School of Earth and Atmospheric Sciences, Georgia Institute of Technology, 311 Ferst Drive, Atlanta, GA 30332-0340 USA. (dufek@gatech.edu)

L. Karlstrom and M. Manga, Department of Earth and Planetary Sciences, University of California, 307 McCone Hall, Berkeley, CA 94720, USA. (leif@berkeley.edu; manga@seismo.berkeley.edu)